EFFECTS OF PHOTOMETRIC REDSHIFT UNCERTAINTIES ON WEAK-LENSING TOMOGRAPHY

Zhaoming Ma, Wayne Hu, and Dragan Huterer

Kavli Institute for Cosmological Physics and Department of Astronomy and Astrophysics, University of Chicago,
5640 South Ellis Avenue, Chicago, IL 60637; mzm@oddjob.uchicago.edu

ABSTRACT

We perform a systematic analysis of the effects of photometric redshift uncertainties on weak-lensing tomography. We describe the photo-z distribution with a bias and Gaussian scatter that are allowed to vary arbitrarily between intervals of $\delta z = 0.1$ in redshift. While the mere presence of bias and scatter does not substantially degrade dark energy information, uncertainties in both parameters do. For a fiducial next-generation survey each would need to be known to better than about 0.003–0.01 in redshift for each interval in order to lead to less than a factor of 1.5 increase in the dark energy parameter errors. The more stringent requirement corresponds to a larger dark energy parameter space, when redshift variation in the equation of state of dark energy is allowed. Of order 10^4–10^5 galaxies with spectroscopic redshifts fairly sampled from the source galaxy distribution will be needed to achieve this level of calibration. If the sample is composed of multiple galaxy types, a fair sample would be required for each. These requirements increase in stringency for more ambitious surveys; we quantify such scalings with a convenient fitting formula. No single aspect of a photometrically binned selection of galaxies such as their mean or median suffices, indicating that dark energy parameter determinations are sensitive to the shape and nature of outliers in the photo-z redshift distribution.

Subject headings: cosmology: theory — gravitational lensing — large-scale structure of universe

Online material: color figures

1. INTRODUCTION

Weak gravitational lensing of galaxies by large-scale structure is rapidly becoming one of the most powerful cosmological probes (Bartelmann & Schneider 2001; Refregier 2003). Following the first detections a few years ago (Van Waerbeke et al. 2000; Kaiser et al. 2000; Bacon et al. 2000; Wittman et al. 2000; Refregier et al. 2004), weak lensing has produced increasingly better constraints on the matter density relative to critical Ω_m and the amplitude of mass fluctuations σ_8 (Hoekstra et al. 2002; Pen et al. 2002, 2003; Brown et al. 2003; Jarvis et al. 2003; Heymans et al. 2005; Van Waerbeke et al. 2005). While weak lensing is most sensitive to the amount and distribution of dark matter, it also has the potential to probe the dark energy through its effect on the growth of structure and distances (Hu & Tegmark 1999; Huterer 2002; Hu 2002b; Takada & Jain 2004; Song & Knox 2004; Ishak 2005). Indeed, when combined with other cosmological probes, weak-lensing data already produce interesting constraints on the dark energy (Jarvis et al. 2005).

By utilizing source galaxy redshifts to study the growth of structure and the distance-redshift relation tomographically, substantially more dark energy information can be recovered (Hu 1999). In fact, future weak-lensing surveys such as PanSTARRS,[1] Supernova/Acceleration Probe[2] (SNAP; Aldering et al. 2004), and Large Synoptic Survey Telescope[3] (LSST) are expected to impose constraints on dark energy that are comparable to those from Type Ia supernovae (see, e.g., Refregier et al. 2004). In the more near term, the Canada-France-Hawaii Telescope Legacy Survey[4] (CFHTLS) and the Dark Energy Survey[5] are expected to help bridge the gap between the current and ambitious future surveys.

Powerful future surveys will require a much more stringent control of the systematics. Recent work has addressed systematic errors from the computation of the nonlinear power spectrum (Vale & White 2003; White & Vale 2004; Heitmann et al. 2005; Huterer & Takada 2005; Hagan et al. 2005), baryonic cooling and pressure forces on the distribution of large-scale structures (White 2004; Zhan & Knox 2004), approximations in inferring the shear from the maps (Dodelson & Zhang 2005; White 2005), and the presence of dust (Vale et al. 2004). Such studies have stimulated work on how to improve the point-spread function (PSF) reconstruction (Jarvis & Jain 2004), estimate shear from noisy maps (Bernstein & Jarvis 2002; Hirata & Seljak 2003; Hoekstra 2004), and protect against the small-scale biases in the power spectrum (Huterer & White 2005).

In this work we consider the effect of errors in photometric redshifts of source galaxies on weak-lensing tomography. Of course, the total number of galaxies, which is currently in the millions and might be in the billions with future surveys, is too large for spectroscopic measurements to be feasible. One therefore needs to rely on the photometric redshifts whose accuracy with the current state of the art in photometry, algorithms, galaxy classification, etc., while presently adequate, may not be sufficient for future surveys that are expected to have very small statistical errors. Uncertain photometric redshifts blur the tomographic bin divisions of source galaxies. In the extreme case when photometric redshift errors are comparable to the width of the distribution itself, one completely loses tomographic information, degrading the cosmological parameter accuracies by up to an order of magnitude.

In this paper we study how the photometric redshift uncertainties affect cosmological parameter determinations. We construct an explicit mapping between the photometric and true redshifts and parameterize it to allow an arbitrary evolution of the bias and scatter between discrete redshift intervals. We then study how accurately the photometric redshifts need to be known a priori and, in particular, which details of the photometric redshift

---

[1] See http://pan-starrs.ifa.hawaii.edu.
[2] See http://snap.lbl.gov.
[3] See http://www.lsst.org.
[4] See http://www.cfht.hawaii.edu/Science/CFHLS.
[5] See http://cosmology.astro.uiuc.edu/DES.

error distribution are the main source of degeneracy with cosmological parameters. We hope that this study will help stimulate work on assessing and improving existing algorithms for photometric redshift estimation (e.g., C. E. Cunha et al. 2005, in preparation).

The outline of the paper is as follows. In § 2 we introduce the formalism and parameterizations of both cosmology and photometric redshift errors. We explore the loss of lensing information on the dark energy to photometric redshift uncertainties in § 3. We show how this lost information is regained as we impose prior knowledge of the photometric redshift parameters in § 4. We discuss our results and conclude in § 5.

2. METHODOLOGY

In this section we discuss the modeling of the photometric redshift distribution. We then illustrate the flexibility of this description through two different fiducial models for the distribution. Finally, we discuss its relationship to lensing observables and the Fisher formalism for addressing its impact on parameter estimation.

2.1. *Photo-z Distribution*

Having only the photometric redshift ("photo-z") of the source galaxies at hand, the observer will necessarily bin the galaxies by their photometric redshifts z_{ph} rather than true (spectroscopic) redshifts z. With a probability distribution $p(z_{ph}|z)$ in z_{ph} at a given z, the true redshift distributions of the bins necessarily overlap.

In general, this distribution can vary arbitrarily with z. The true distribution of galaxies $n_i(z)$ that fall in the ith photo-z bin with $z_{ph}^{(i)} < z_{ph} < z_{ph}^{(i+1)}$ becomes

$$n_i(z) = \int_{z_{ph}^{(i)}}^{z_{ph}^{(i+1)}} dz_{ph}\, n(z) p(z_{ph}|z). \tag{1}$$

Here $n(z) = d^2N/dz\, d\Omega$ is the overall galaxy redshift distribution and is chosen to have the form

$$n(z) \propto z^\alpha \exp\left[-(z/z_0)^\beta\right]. \tag{2}$$

Unless otherwise stated, we adopt $\alpha = 2$, $\beta = 2$ and fix z_0 such that median redshift is $z_{med} = 1$. The total number of galaxies per steradian

$$n^A = \int_0^\infty dz\, n(z) \tag{3}$$

fixes the normalization, and we analogously define

$$n_i^A = \int_0^\infty dz\, n_i(z) \tag{4}$$

for the bins.

By construction, the sum of the individual distributions equals the total $\Sigma_i n_i(z) = n(z)$. Therefore, regardless of how complicated the photo-z probability distribution gets and hence the redshift distributions of the tomographic bins, the total distribution of galaxies $n(z)$ is unchanged.

This construction cleanly separates uncertainties due to the photometric redshifts of the individual survey galaxies characterized by $p(z_{ph}|z)$ from uncertainties in the redshift distribution of the underlying total distribution of galaxies $n(z)$. We mainly

consider the former in this work but comment on the latter in § 5 (see also Huterer et al. 2005; Ishak & Hirata 2005). The rationale is that even without any knowledge of the photo-z's of the survey galaxies themselves, one can at least bin all of the galaxies together assuming that the underlying redshift distribution or selection function of the survey is known. In practice, this means that one must obtain information about the underlying distribution from an independent source (say, another survey through a study of the luminosity function) or from a fair subsample of survey galaxies with spectroscopic redshifts.

2.2. *Photo-z Models*

Any photo-z model may be described by providing a function for the distribution of photometric redshifts given the true redshift, $p(z_{ph}|z)$. For the purposes of this paper we take the simplifying assumption that this function is a Gaussian at each redshift, i.e.,

$$p(z_{ph}|z) = \frac{1}{\sqrt{2\pi}\sigma_z} \exp\left[-\frac{(z - z_{ph} - z_{bias})^2}{2\sigma_z^2}\right]. \tag{5}$$

However, we allow the bias $z_{bias}(z)$ and scatter $\sigma_z(z)$ to be arbitrary functions of redshift. The redshift distribution of the tomographic bins defined by equation (1) can then be written as

$$n_i(z) = \tfrac{1}{2} n(z)[\text{erf}\,(x_{i+1}) - \text{erf}\,(x_i)], \tag{6}$$

with

$$x_i \equiv \left(z_{ph}^{(i)} - z + z_{bias}\right)/\sqrt{2}\sigma_z, \tag{7}$$

where erf (x) is the error function.

The Gaussian assumption is not as restrictive as it might naively seem. By allowing the bias and scatter to be arbitrary functions of redshift, one can obtain arbitrarily complex redshift distributions in the tomographic bins through equation (1). In fact, the mapping is in principle completely general for finite bins and a smooth underlying distribution. Galaxies in a finite range of redshift over which the distribution is nearly constant can then be mapped to any z_{ph}.

In practice we represent the free functions $z_{bias}(z)$ and $\sigma_z(z)$ with a discrete set of N_{pz} photo-z parameters. They represent the values of the functions at z_μ that are equally spaced from $z = 0$ to 3. To evaluate the functions at an arbitrary redshift, we take a linear interpolation of the discrete parameters in redshift.

While a finite N_{pz} does restrict the form of the distribution, it still allows radically different redshift distributions given the same tomographic bins. For example, consider two different photo-z models:

1. Model I: $z_{bias}(z) = 0$; $\sigma_z(z) = 0.05(1 + z)$.
2. Model II: $z_{bias}(z) = 0$; $\sigma_z(z) = 0.2$ for $z < 1.0$ and $\sigma_z(z) = 0.5$ for $z > 1.0$.

The distribution $p(z_{ph}|z)$ is illustrated in Figure 1 for $N_{pz} = 31$ through the 1 σ scatter region. The resulting redshift distributions for $N_{div} = 5$ tomographic bins are shown in Figure 2. These specific choices of N_{pz} and N_{div} are motivated in § 3.

Model II demonstrates that sharp changes in the Gaussian photometric parameters can map neighboring galaxies in redshift to quite different tomographic bins. The redshift distributions of the bins can thus have features that are sharper than the assumed scatter. Additionally, photo-z degeneracies that take two distinct spectroscopic redshift ranges into a single photometric redshift
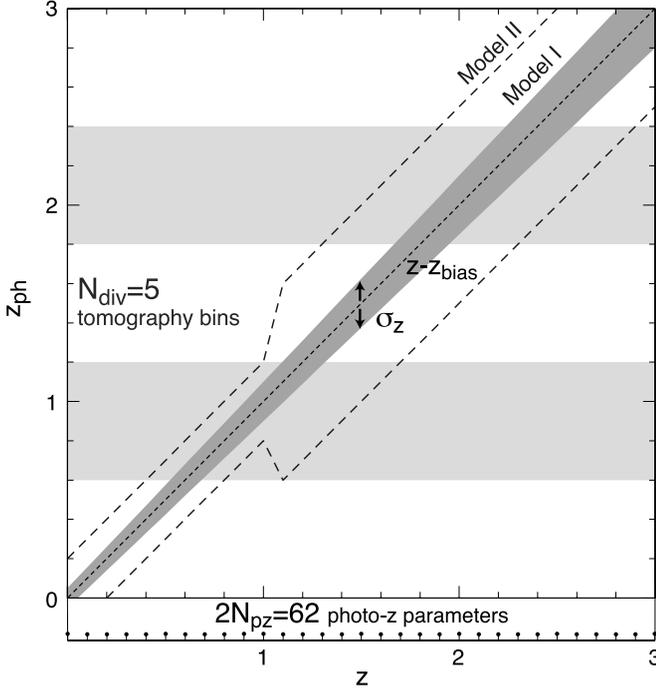
FIG. 1.—Parameterization of the photo-z distribution and two illustrative fiducial models. The distribution spreads galaxies at a given redshift z into a distribution in z_{ph} characterized here by a bias z_{bias} and a scatter σ_z whose evolution is parameterized by interpolating their values at N_{pz} redshifts z_μ. In both models $z_{bias} = 0$, whereas σ_z, given in § 2.2, is illustrated here for model I (*shaded region*) and model II (*dashed lines*) as 1 σ bands. Galaxies binned according to their photometric redshifts (N_{div} horizontal bands) then have overlapping redshift distributions determined by the $2N_{pz}$ photo-z parameters. [*See the electronic edition of the Journal for a color version of this figure.*]

and lead to bimodality in the binned distribution can be modeled by a large z_{bias}. Finally, galaxy types with different photo-z distribution at a given redshift can be approximated by discontinuous jumps between infinitesimally spaced redshift bins. Such considerations, while potentially important, are beyond the scope of this work.

In summary, allowing our set of parameters to freely vary, one can access a wide range of tomographic redshift distributions. Uncertainty in these parameters will then cause uncertainties in tomographic dark energy determinations.

2.3. *Lensing Observables*

The convergence power spectrum at a fixed multipole l and for the ith and jth tomographic bin $P_{ij}^\kappa(l)$ is given by (Kaiser 1992, 1998)

$$n_i^A n_j^A P_{ij}^\kappa(l) = \int_0^\infty dz\, W_i(z) W_j(z) \frac{H(z)}{D^2(z)} P(k_l,\, z), \quad (8)$$

where $H(z)$ is the Hubble parameter and $D(z)$ is the angular diameter distance in comoving coordinates. $P(k_l,\, z)$ is the three-dimensional matter power spectrum and $k_l = l/D(z)$ is the wavenumber that projects onto the multipole l at redshift z. The weights W are given by

$$W_i(z) = \frac{3}{2}\Omega_m \frac{H_0^2 D(z)}{H(z)}(1+z)\int_z^\infty dz'\, n_i(z')\frac{D_{LS}(z,\, z')}{D(z')}, \quad (9)$$

where $D_{LS}(z,\, z')$ is the angular diameter distance between the two redshifts. The power spectrum is computed from the transfer
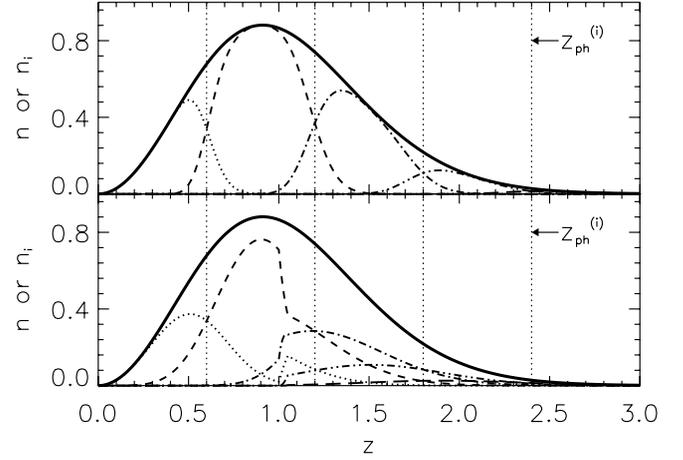
FIG. 2.—Source galaxy redshift distribution $n(z)$. *Top*: Photo-z model I. *Bottom*: Photo-z model II. The solid line is the overall galaxy distribution defined in eq. (2). The other lines are the true (spectroscopic) distributions that correspond to the sharp divisions in photo-z space (denoted by dotted vertical lines). [*See the electronic edition of the Journal for a color version of this figure.*]

function of Eisenstein & Hu (1999) with dark energy modifications from Hu (2002a) and the nonlinear fitting function of Peacock & Dodds (1996).

With tomographic binning, the number-weighted power spectrum $n_i^A n_j^A P_{ij}^\kappa$ and not P_{ij}^κ is the fundamental observable. Even given photometric redshift uncertainties in the binning, it is always possible to recover the total weighted power spectrum (Hu 1999)

$$\left(n^A\right)^2 P^\kappa = \sum_{i,j=1}^{N_{div}} n_i^A n_j^A P_{ij}^\kappa, \quad (10)$$

since the weighting is based on the observed n_i^A. By treating $n_i^A n_j^A P_{ij}^\kappa$ as the observable, one guarantees that the addition of photo-z estimates for the individual galaxies can only add information. This would not be true if P_{ij}^κ were taken as the only observable quantity. Given that changes in photo-z parameters induce changes in n_i^A, the binned power spectra P_{ij}^κ do not contain enough information to weight the power spectra and recover the total P^κ.

That the binned angular number densities n_i^A are observed quantities also implies that there is additional direct information on the photo-z parameters that does not depend on shear measurements. For example, a high fraction of galaxies in bins with z_{ph} larger than the median redshift would imply a large photo-z bias. We choose not to consider this sort of information since it is not directly related to lensing. Furthermore, for the small changes in n_i^A that we will typically be considering, the sample variance between the observed n_i^A and that predicted by the underlying redshift distribution and the photo-z parameters cannot be ignored (Hu & Kravtsov 2003). Therefore, we consider the number-weighted power spectra $n_i^A n_j^A P_{ij}^\kappa$ as the fundamental lensing observables.

2.4. *Fisher Matrix*

The Fisher matrix quantifies the information contained in the lensing observables

$$O_{a=i(i-1)/2+j}(l) = n_i^A n_j^A P_{ij}^\kappa(l) \quad (i \geq j) \quad (11)$$

on a set of cosmological and photo-z parameters p_μ. Under the approximation that the shear fields are Gaussian out to l_{max}, the Fisher matrix is given by

$$F_{\mu\nu} = \sum_{l=2}^{l_{max}} (2l+1) f_{sky} \sum_{ab} \frac{\partial O_a}{\partial p_\mu} \left[\boldsymbol{C}^{-1}\right]_{ab} \frac{\partial O_b}{\partial p_\nu}, \quad (12)$$

so that the errors on the parameters are given by $\Delta p_\mu = [\boldsymbol{F}^{-1}]_{\mu\mu}^{1/2}$.

Given shot and Gaussian sample variance, the covariance matrix of the observables becomes

$$C_{ab} = n_i^A n_j^A n_k^A n_l^A \left(P_{ik}^{tot} P_{jl}^{tot} + P_{il}^{tot} P_{jk}^{tot} \right), \quad (13)$$

where $a = i(i-1)/2 + j$, $b = k(k-1)/2 + l$. The total power spectrum is given by

$$P_{ij}^{tot} = P_{ij}^\kappa + \delta_{ij} \frac{\gamma_{int}^2}{n_i^A}, \quad (14)$$

where γ_{int} is the rms shear error per galaxy per component contributed by intrinsic ellipticity and measurement error. For illustrative purposes we use $l_{max} = 3000$, f_{sky} corresponding to 4000 deg^2, $\bar{n}^A$ corresponding to 55 galaxies arcmin^{-2}, and $\gamma_{int} = 0.4$. The value of l_{max} is motivated by simulations that find substantial deviations from Gaussianity and weak-lensing approximations on arcminute scales (White & Hu 2000; Vale & White 2003). For our choice of noise parameters above, the results are insensitive to l_{max} since the measurements are noise dominated on those scales.

For the cosmological parameters, we consider four parameters that affect the matter power spectrum: the physical matter density $\Omega_m h^2$ (=0.14), physical baryon density $\Omega_b h^2$ (=0.024), tilt n_s (=1), and the amplitude δ_ζ (=5.07 × 10^{-5}; or $A = 0.933$; Spergel et al. 2003). Values in parentheses are those of the fiducial model. Unless otherwise stated, we take priors on these four parameters of $\Delta \ln \Omega_m h^2 = \Delta \ln \Omega_b h^2 = \Delta \ln \delta_\zeta = \Delta n_s = 0.05$. These priors represent only a modest improvement over current determinations. Our results on the relative degradation in constraints caused by photo-z errors are insensitive to reasonable variations in this choice.

To these four cosmological parameters, we add either two or three dark energy parameters: the dark energy density Ω_{DE} (=0.73), its equation of state today $w_0 = p_{DE}/\rho_{DE}|_{z=0}$ (=−1), and optionally its derivative $w_a = -dw/da|_{z=0}$ (=0) assuming a linear evolution with the scale factor $w = w_0 + (1-a)w_a$.

Note that throughout this paper our notational convention is Latin indices for tomographic bins and Greek indices for parameters.

3. DARK ENERGY INFORMATION LOSS

In this section we consider the nature of the tomographic information on the dark energy and its loss to photo-z uncertainties. We establish the maximal information that can be gained through tomographic redshift divisions for a given dark energy parameterization. We then determine the number of photo-z degrees of freedom that would be required to lose this information. This loss of information is caused by a degeneracy between cosmological and photo-z parameters. We explicitly construct an example of this degeneracy as both an illustration and test of our statistical methodology.

3.1. *Maximal Information and N_{div}*

For any given choice of dark energy parameterization, the information contained in lensing will saturate with some finite
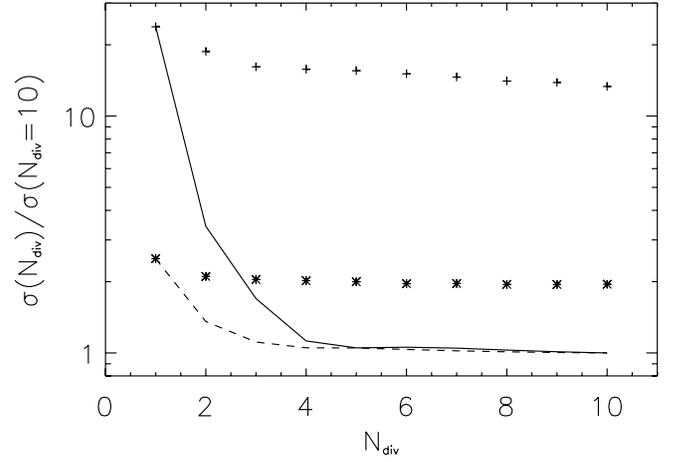
Fig. 3.—Relative errors in dark energy parameters as a function of the number of tomographic divisions N_{div}. Solid lines correspond to w_a for the set $\{w_0, w_a, \Omega_{DE}\}$; dashed lines to w_0 for $\{w_0, \Omega_{DE}\}$. Both lines assume that all photo-z parameters are perfectly known (i.e., fixed). Note that the results converge at smaller N_{div} for a smaller dark energy space and that $N_{div} = 5$ is more than sufficient in either case. The symbols correspond to the same cases, but now with $2N_{pz} = 62$ photo-z parameters marginalized (photo-z priors of $\Delta \sigma_z = \Delta z_{bias} = 10$ are applied). Here essentially all tomographic information is lost so that the errors are comparable to those of $N_{div} = 1$ or no tomography. [*See the electronic edition of the Journal for a color version of this figure.*]

number of tomographic bins N_{div} (Hu 1999). Since the broad lensing kernel of equation (9) makes the shear for neighboring source redshifts highly correlated, most of the information is contained in a few coarse bins. The exact number depends on the type of information that is to be extracted. Roughly speaking, the number of bins should exceed the number of dark energy parameters.

Figure 3 (*lines*) quantifies this expectation through improvement in the errors on dark energy parameters as a function of N_{div} for model I. For a two-parameter dark energy space $\{w_0, \Omega_{DE}\}$, $N_{div} = 3$ divisions equally spaced from $z = 0$ to 3 are enough for the improvements in w_0 to saturate. For a three-parameter dark energy space $\{w_0, w_a, \Omega_{DE}\}$, $N_{div} = 4$ divisions are sufficient for w_a. Note that $N_{div} = 1$ corresponds to no tomography or no photo-z information on the individual galaxies. The dark energy parameters that are not shown in Figure 3 behave similarly. In what follows we conservatively adopt $N_{div} = 5$ as sufficient to extract the dark energy information. With $N_{div} = 5$ and photo-z parameters fixed, the constraints on dark energy parameters are shown in Table 1.

Note that improvements relative to the no-tomography case are more significant in the larger parameter space. This is due to the fact that w_0 is nearly degenerate with w_a since lensing mainly constrains $w(z)$ at some intermediate redshift (see below). Even the small amount of information in the fine-binned tomography assists the breaking of the degeneracy.

3.2. *Maximal Degradation and N_{pz}*

Next we choose the number of photo-z parameters N_{pz} that describe each of the functions $z_{bias}(z)$ and $\sigma_z(z)$. We seek to allow enough freedom in the photo-z parameters so that in the absence of prior information on their values all of the tomographic information is lost. Because the limit of no tomographic information corresponds to $N_{div} = 1$, we have a quantitative means of assessing the minimal N_{pz}. When N_{pz} becomes large enough, the variations in redshift, which act on the characteristic scale of

TABLE 1
BASELINE CONSTRAINTS ON DARK ENERGY PARAMETERS

Photo-z Model	Parameters	$\sigma(\Omega_{DE})$	$\sigma(w_0)$	$\sigma(w_a)$
I	$\{\Omega_{DE}, w_0\}$	0.0062	0.061	. . .
	$\{\Omega_{DE}, w_0, w_a\}$	0.024	0.25	0.69
II	$\{\Omega_{DE}, w_0\}$	0.0073	0.070	. . .
	$\{\Omega_{DE}, w_0, w_a\}$	0.034	0.36	0.96

$\delta z = 3.0/(N_{pz} - 1)$, are rapid enough that they do not mimic any variation in cosmological parameters.

Figure 4 shows the degradation in the errors on w_a for the cases of $N_{pz} = 6, 11, 21, 31$, and 61 as a function of the prior on the photo-z parameters. Results for w_0 are similar. To compare priors for different N_{pz} values, we have here rescaled the individual parameter priors by $(N_{pz}/31)^{1/2}$ so as to be equal for a fixed redshift interval $\delta z = 0.1$. The results have converged with $N_{pz} \geq 21$. To be conservative, in the rest of this paper we use $N_{pz} = 31$, or a total of 62 photo-z parameters.

The impact of this choice of $N_{pz} = 31$ as a function of N_{div} for dark energy parameters is shown in Figure 3 (*symbols*). For all N_{div}, these constraints match those with no tomographic binning very well, showing that without prior information on the photo-z parameters all tomographic information has been effectively destroyed and we recover the case with a single redshift division. The small discrepancy comes from the inadequacies in the Fisher matrix, one of which is the local approximation to the parameter errors, as we discuss in the next section.

3.3. *Photo-z–Dark Energy Degeneracy*

With a sufficient number of unknown photo-z parameters $2N_{pz} \gtrsim 62$, the Fisher matrix results of the previous section imply that dark energy information in tomography is completely lost. This fact implies that there is a nearly perfect degeneracy between photo-z, dark energy, and other cosmological parameters. Here we examine that aspect of the degeneracy that involves the photo-z and dark energy parameters only. This degeneracy alone suffices to destroy most of the tomographic information and will remain even if the other cosmological parameters are perfectly measured from other sources.

Constructed from parameter derivatives, the Fisher matrix is a local expression of the degeneracy in parameter space. Because the Fisher matrix results imply that the degeneracy persists to large changes in the dark energy parameters, it is important to assess the extent of the degeneracy more directly and test the validity of the Fisher approximation. If the degeneracy relation "curves" in parameter space, the Fisher approximation will only find the local tangent.

We start by identifying this local tangent with the Fisher matrix. To isolate the degeneracy between dark energy and photo-z parameters, we eliminate the other cosmological parameters, formally by adding strong priors to the Fisher matrix. For numerical reasons we also add a weak prior on photo-z parameters ($\Delta z_{bias} = \Delta \sigma_z = 1$) to control numerical errors from the nearly singular Fisher matrix. Of the eigenvectors of this Fisher matrix that involve the dark energy, those with the smallest eigenvalues will be responsible for most of the photo-z dark energy degeneracy. We find that a single linear combination of parameters (dark energy *and* photo-z) contributes most ($\sim$98%) of the errors in dark energy parameters w_0 and w_a. Thus, the degeneracy is essentially one-dimensional in the multidimensional parameter space. Let us call this direction, or the eigenvector of the Fisher matrix, $\boldsymbol{e}_w$.
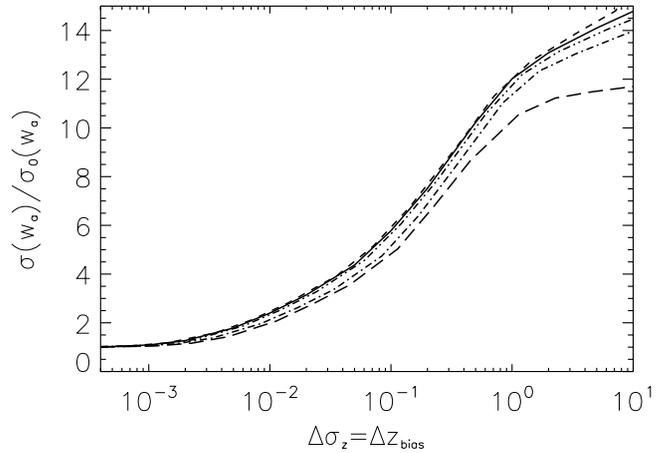
FIG. 4.—Error degradations in w_a (that is, errors in w_a relative to the error with perfect knowledge of photo-z parameters) as a function of the photo-z prior. The photo-z priors are rescaled by a factor of $(N_{pz}/31)^{1/2}$ so that they reflect constraints per $\delta z = 0.1$ independently of N_{pz}. Different lines from top to bottom correspond to different N_{pz}: 61 (*short-dashed line*), 31 (*solid line*), 21 (*double-dot–dashed line*), 11 (*dot-dashed line*), and 6 (*long-dashed line*). Note that the results have converged with $N_{pz} \geq 21$; we use $N_{pz} = 31$ just to be conservative. [*See the electronic edition of the Journal for a color version of this figure.*]

The true extent of the degeneracy is quantified by the change in χ^2 between the fiducial model p_μ and a trial model $\tilde{p}_\mu$,

$$\Delta\chi^2_{true} = \sum_{l=2}^{l_{max}} (2l+1) f_{sky} \sum_{ab} \left[O_a(l; p_\mu) - O_a(l; \tilde{p}_\mu) \right]$$
$$\times \left[\boldsymbol{C}^{-1} \right]_{ab} \left[O_b(l; p_\mu) - O_b(l; \tilde{p}_\mu) \right]. \quad (15)$$

If the Fisher matrix approximation were valid out to, say, 1 σ along the degeneracy, then the trial model $\tilde{p}_\mu = p_\mu + \sigma_w \boldsymbol{e}_w$, where σ_w^{-2} is the eigenvalue corresponding to $\boldsymbol{e}_w$, would be separated by

$$\Delta\chi^2_F = \sigma_w^2 \boldsymbol{e}_w^T \boldsymbol{F} \boldsymbol{e}_w = 1, \quad (16)$$

due to the orthonormality of the eigenvectors. In practice, $\Delta\chi^2_{true} = 857$ for this extrapolation, indicating a curvature in the degeneracy direction. In other words, p_μ and $\tilde{p}_\mu$ are highly distinguishable models in spite of the Fisher prediction that they are indistinguishable.

Even given curvature in the degeneracy direction, the Fisher approximation remains useful if it accurately predicts the extent of the degeneracy. This is especially true if the curvature lies mainly in the photo-z nuisance parameters, which exist only to be marginalized. To assess the extent of the degeneracy, we use the Fisher matrix as a local approximation of the degeneracy with the following procedure. Starting at the fiducial model, calculate the Fisher matrix and find $\boldsymbol{e}_w$ as defined above, then take a *small* step along the $\boldsymbol{e}_w$ direction. Now calculate the Fisher matrix at the new point, find the new $\boldsymbol{e}_w$, and take another small step along this new direction. Repeat. The smallness of the steps is controlled such that the change of χ^2 between steps agrees within 10% with that predicted by the Fisher matrix. This 10% error may add up to a much bigger percentage after a few steps. To make sure that we stay on the degeneracy direction, local minimum of $\Delta\chi^2_{true}$ is searched after a few steps out.

From this construction we find that the extent of the degeneracy in w is accurately predicted by the Fisher matrix. Figure 5 shows that the model with $\Delta\chi^2_F = 1$ (*thick dashed line*) is almost identical to the model with $\Delta\chi^2_{true} = 1$ (*thick solid line*) in $w(z)$.
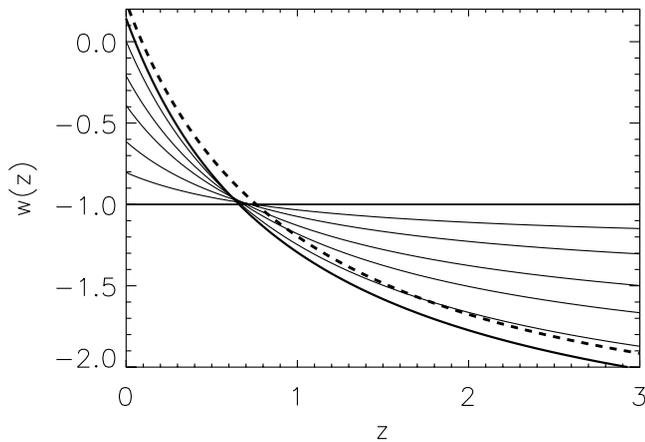
FIG. 5.—Equations of state of dark energy $w(z)$ that are degenerate with photo-z parameters. Solid lines show a series of degenerate models stepping out by $\Delta w_0 = 0.2$ and ending at a model with $\Delta w_0 = 1.14$, which deviates from the fiducial model at $+1\,\sigma$ for the fiducial survey. The tight correlation between w_0 and w_a along the degeneracy direction results in the tight "waist" or pivot where $w(z)$ remains well determined. The dashed line shows that the $+1\,\sigma$ degenerate model as predicted by the Fisher matrix is in good agreement with the true degeneracy even out to large Δw_0. [*See the electronic edition of the Journal for a color version of this figure.*]

In Figure 5 we also show intermediate models along the degeneracy with $\Delta \chi^2_{\text{true}} < 1$. That they all pass through essentially a single point in $w(z)$ space is another indication that the degenerate direction lies almost entirely along a specific linear combination of dark energy parameters as predicted by the Fisher matrix. The curvature in parameter space mainly involves the photo-z parameters.

The redshift at which these lines intersect is $z \approx 0.7$, and at this redshift measurements of w are essentially immune to photometric redshift errors. This immunity reflects the fact that even without tomography lensing can constrain the equation of state at some effective redshift. With two parameters to describe $w(z)$, there is only one remaining linear combination to be affected by photometric redshifts. With a more general parameterization of $w(z)$ we expect that there will be multiple degenerate directions with roughly the same single aspect of $w(z)$ preserved.

Furthermore, the two estimates (true and Fisher) agree on the amplitude of the photo-z parameter variation along the degenerate direction. For example, as shown in Figure 6, at a point along the e_w direction that is $1\,\sigma$ away from the fiducial model, the Fisher matrix indicates that the photo-z parameters changed by $\delta z_{\text{bias}} < 0.06$ and $\delta \sigma_z < 0.07$, while the actual bounds on the variations are $\delta z_{\text{bias}} < 0.04$ and $\delta \sigma_z < 0.07$. Note that these changes are fairly small and imply that subtle variations in the redshift distributions for the tomographic bins are responsible for a degeneracy that degrades errors in w_0 and w_a by an order of magnitude. Figure 6 also shows the difference between these distributions for $\Delta \chi^2_{\text{true}} = 1$. We expect that with a change in the photo-z model, the specific photo-z variations that establish this degeneracy will change, but a strong degeneracy will remain.

In summary, we find that the Fisher matrix is an adequate tool for assessing the existence and extent of degeneracies between photo-z and dark energy parameters. It should not, however, be used to infer the specific changes in the photo-z parameters that establish the degeneracy.

4. PHOTO-z INFORMATION RECOVERY

In the previous section we established the existence of a degeneracy between photo-z parameters and dark energy parame-
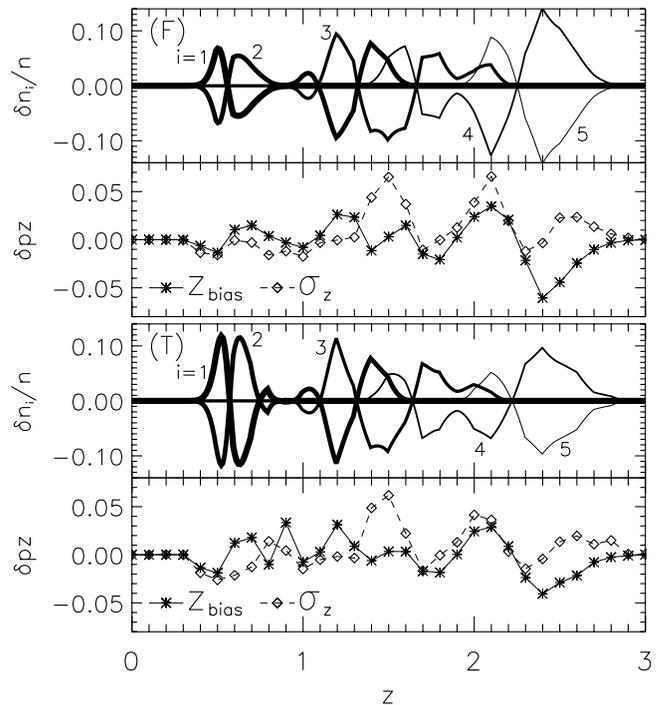
FIG. 6.—Comparison of the fractional differences of the redshift distribution $\delta n_i/n$ in each of the $i = 1, \ldots, 5$ tomographic bins that establishes the $1\,\sigma$ degeneracy with dark energy parameters of an extent $\Delta w_0 \sim 1$. Also shown are the changes in the two sets of discrete photo-z parameters $\delta pz = (\delta \sigma_z, \ \delta z_{\text{bias}})$ that cause these differences, connected by lines to guide the eye. *Top*: Fisher approximation for the $1\,\sigma$ degeneracy. *Bottom*: True degeneracy. [*See the electronic edition of the Journal for a color version of this figure.*]

ters and tested the validity of the local Fisher matrix approximation to this degeneracy. In this section we use the Fisher matrix formalism to investigate the extent to which prior information on the photo-z distributions helps recover the tomographic dark energy information. We assume $2N_{\text{pz}} = 62$ photo-z parameters and $N_{\text{div}} = 5$ tomographic bins throughout this section (see § 3).

4.1. *Photo-z Priors*

We now explore the effect on dark energy parameter constraints of priors on each of the photo-z parameters $z_{\text{bias}}(z_\mu)$ and $\sigma_z(z_\mu)$. For simplicity, we begin by applying a redshift-independent prior on the parameters. In practice, parameters controlling the distributions well above and well below the median redshift require weaker priors. We discuss this point in § 4.3.

Figure 7 shows the error degradation in w_0 assuming the $\{w_0, \Omega_{\text{DE}}\}$ parameterization (*left panel*) and w_a assuming the $\{w_0, w_a, \Omega_{\text{DE}}\}$ parameterization (*right panel*). For reference the baseline errors for the fiducial survey are listed in Table 1.

As in the previous section where other cosmological parameters were artificially fixed, we find that the larger dark energy parameter space is more susceptible to photo-z errors. For example, for the extreme case of no photo-z information, i.e., very weak priors on both bias and scatter parameters, dark energy parameters of the $\{w_0, \Omega_{\text{DE}}\}$ parameterization are degraded by about a factor of 2 while those of $\{w_0, w_a, \Omega_{\text{DE}}\}$ parameterization are degraded by about a factor of 10.

In the more relevant case where we demand that the dark energy error degradation be no larger than 1.5, the requirement per photo-z parameter is about 0.01 for $\{w_0, \Omega_{\text{DE}}\}$ and 0.003 for the $\{w_0, w_a, \Omega_{\text{DE}}\}$ parameterization. Figure 7 also shows that both bias and scatter parameters are important and that knowledge
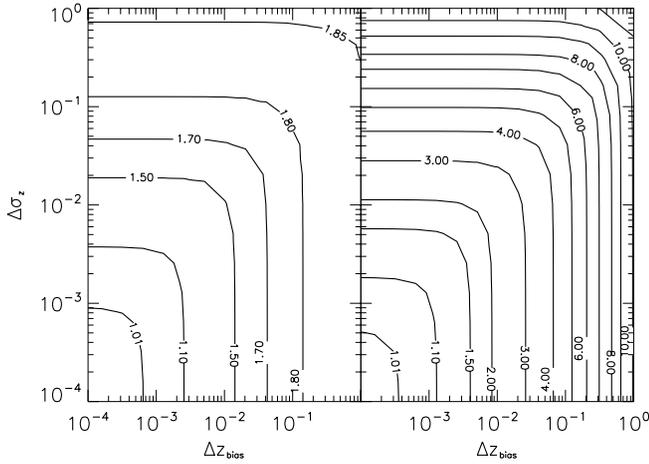
FIG. 7.—Error degradations for constant w_0 (*left*) and those for w_a when both w_0 and w_a are varied (*right*), as a function of photo-z parameter priors. Here the degradations are defined as actual errors relative to errors that assume the photo-z parameters to be perfectly known. Priors on the photo-z parameters $z_{bias}(z_\mu)$ and $\sigma_z(z_\mu)$ are shown on the x-axis and y-axis, respectively. Fiducial photo-z model I is assumed and the photo-z parameter spacing in redshift is $\delta z = 0.1$.

of the bias is only slightly more important than that of the scatter. Furthermore, dark energy parameters that are not shown in Figure 7 have very similar requirements to those plotted in either parameterization.

4.2. *Dependence on Fiducial Model*

The results above are for a specific choice of the fiducial model for the photo-z distribution and survey. To explore the dependence on the former, we take the very different photo-z model II, where the scatter is substantially larger and jumps discontinuously in redshift. Even so, the requirements on the photo-z parameters are very similar; see Figure 8. In particular, within the interesting regime where the photo-z prior is smaller than unity and the degradation in dark energy parameter errors is a factor of a few or lower, the two models agree very well.

On the other hand, photo-z requirements do depend on the parameters f_{sky}, γ_{int}, and n^A that determine the level of sample and noise variance in the survey. The trend is that the more ambitious the survey, the more stringent the requirements on photo-z

parameters. The scaling for the priors on photo-z parameters can roughly be described as

$$\frac{\Delta p(f_{sky},\ \gamma_{int},\ n^A,\ d)}{\Delta p(0.1,\ 0.4,\ 55,\ 1.5)} = \frac{g(d)}{g(1.5)}\sqrt{\frac{0.1}{f_{sky}}}\left[1 + C\left(\frac{\gamma_{int}^2}{0.16}\frac{55}{n^A} - 1\right)\right],$$
(17)

where $\Delta p = \Delta z_{bias} = \Delta \sigma_z$ gives the photo-z priors and n^A is in units of arcmin^{-2}. Here $g(d) = \Delta p(0.1,\ 0.4,\ 55,\ d)$ scales the prior requirement to alternate levels of degradation d; it is shown in Figure 8 as $d(g)$ and is only weakly dependent on the fiducial photo-z model. With the best fit $C = 0.6$ this scaling is good up to a factor of 2 for any reasonable set of survey parameters.

Finally, the photo-z precision requirement is not very sensitive to z_{med}, the median source redshift of the survey. For $0.68 < z_{med} < 1.3$, Δp varies by less than 40%.

4.3. *Training Set Size*

The priors on the photo-z parameters ultimately require a training set of galaxies with measured spectroscopic redshifts. Operationally suppose that a photo-z training set has N_{spec}^μ spectroscopic redshifts per redshift interval determined by N_{pz} (here $\delta z = 0.1$).

Given a Gaussian distribution for the photo-z distribution and a fair sample of spectroscopic galaxies selected from this distribution, the training set would independently determine the bias and scatter to

$$\Delta z_{bias}(z_\mu) = \sigma_z(z_\mu)\sqrt{1/N_{spec}^\mu},$$
$$\Delta \sigma_z(z_\mu) = \sigma_z(z_\mu)\sqrt{2/N_{spec}^\mu}.$$
(18)

For a fixed dark energy degradation, N_{spec}^μ depends on two things: the fiducial σ_z and the required prior as scaled from equation (17). Since the photo-z prior requirement is roughly independent of σ_z as shown in Figure 8, the larger the scatter, the larger the required training set. Note that N_{spec} ($\equiv \sum_\mu N_{spec}^\mu$) is robust to changes in the number of photo-z parameters or δz. For example, a binning of $\delta z = 0.05$ would imply twice as many photo-z parameters that would need to be constrained a factor of $\sqrt{2}$ less well, yielding the same requirement on N_{spec}.

For determining the redshift extent of the training set, it is important to go beyond our simple redshift independent prior.

FIG. 8.—Comparison of the photo-z requirements for our two fiducial photo-z models. The solid line shows the degradations for model I, while the dashed line corresponds to model II. The fiducial errors in w_a when the photo-z's are perfectly known are $\sigma_0(w_a) = 0.69$ (model I) and 0.96 (model II).
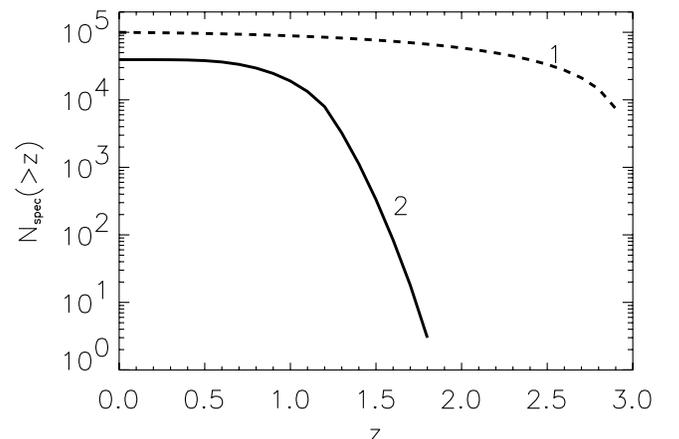
FIG. 9.—Cumulative requirement of N_{spec} for 1.5 dark energy error degradation. The corresponding photo-z prior templates are shown in Fig. 10 with the dashed line as the flat prior and the solid line as the weighted prior.
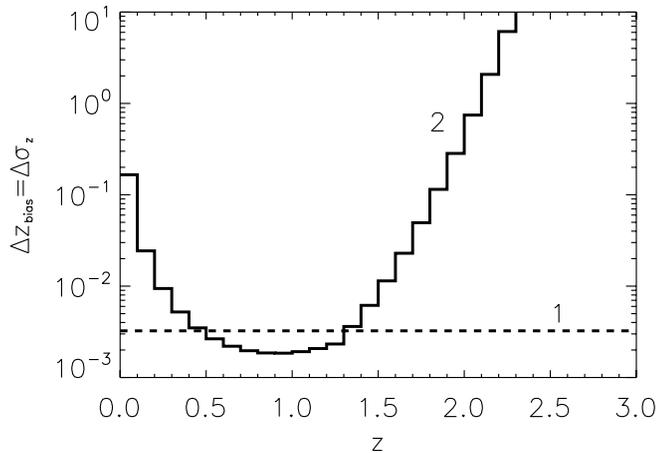
Fig. 10.—Photo-z prior templates of how the bias and scatter priors vary with redshift to produce a fixed error degradation in dark energy parameters. The degradation on w_a is 1.5. The dashed line is the flat template used in Fig. 7. The solid line is the weighted template constructed according to the galaxy number density. At $z < 1.2$ the line follows $\bar{n}_i^{-1}$, while at $z > 1.2$ the line follows $\bar{n}_i^{-3}$. Here $\bar{n}_i$ is the number of galaxies in each redshift interval $\delta z = 0.1$.

Figure 9 shows the cumulative $N_{\text{spec}}(>z)$ required for 1.5 degradation in dark energy. Notice that this flat prior assumption would require a substantial number of galaxies across the whole redshift range (10^5), including 8×10^4 galaxies above $z = 1.5$. This number is artificially high since the actual requirements on the prior fall sharply away from the median redshift of the distribution.

To illustrate the difference, we constructed a weighted template of how the bias and scatter priors vary with redshift to produce a fixed degradation in dark energy parameters. We choose a simple power law of $\bar{n}_i$, which is the number of galaxies in each redshift interval ($\delta z = 0.1$ for the fiducial choice of $N_{\text{pz}} = 31$) corresponding to the photo-z parameters. At $z < 1.2$, the power is chosen as -1. To account for the difficulty in measuring redshifts at $z > 1.5$ from optical bands, we steepen the index to -3 for $z > 1.2$. Figure 10 compares the flat prior to the weighted one. The requirement for the weighted one drops to a total of 4×10^4, but more importantly only 300 at $z > 1.5$.

For dark energy degradations other than 1.5, we provide in Figure 11 the ratio of N_{spec} for an arbitrary dark energy degradation to that of 1.5 degradation. In order to find out the N_{spec} requirement for any dark energy degradation, all one needs to do
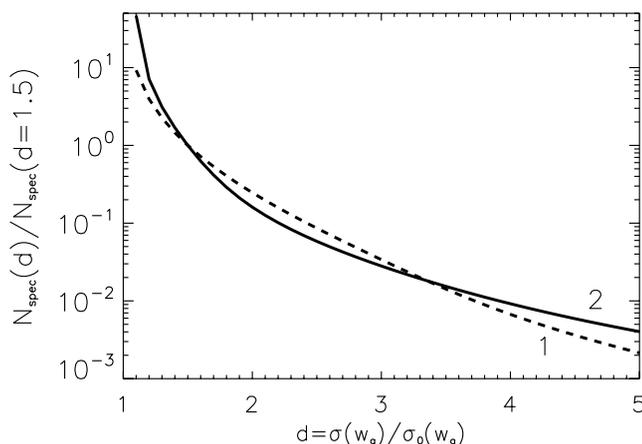
Fig. 11.—Ratio of required N_{spec} for an arbitrary w_a degradation relative to that of 1.5 degradation for the two prior templates of Fig. 10.
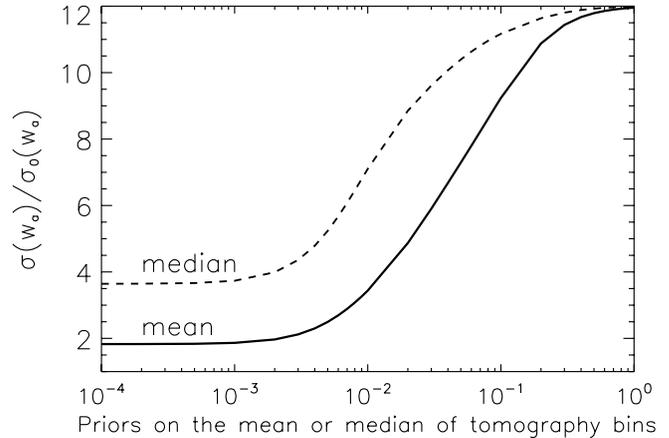
Fig. 12.—Effect of the mean or median of tomography bins. Vertical axis is dark energy error degradation. The solid line and the dashed line are for the case of mean and median, respectively. Photo-z priors of $\Delta\sigma_z = \Delta z_{\text{bias}} = 1$ are assumed.

is to look up the ratio in Figure 11 and multiply it by the N_{spec} in Figure 9.

We have tested that the scaling relation to surveys with different fiducial parameters of equation (17) works equally well for both the flat and weighted priors. Using the scaling relation, the requirement of N_{spec} could be scaled to different surveys easily.

4.4. Mean versus Median

We now estimate the amount of information that comes from knowing the median or mean of the redshift distribution of source galaxies in each tomographic bin. Note that this is distinct from priors on the photo-z bias or mean photo-z at a given redshift. This question is interesting in its own right, but also because other work, parallel to this (Huterer et al. 2005), has parameterized the photo-z uncertainty by the centroids of the tomographic bins, which when varied shift the overall distribution of the corresponding tomographic bin. While one intuitively expects that the centroid of the photo-z bin (or more generally its mean) carries the most information, we now have the tools to precisely examine the relative contribution of the mean relative to that of the higher moments.

Figure 12 shows degradations of the error in w_a as a function of priors on the mean or median of the tomographic bins. All of the photo-z parameters are given a weak prior of unity for numerical stability. A prior of 10^{-3} on the mean is enough to render the mean essentially precisely known. But the dark energy degradation is still a factor of 2 even with perfect mean measurements showing that there remains information lost to the higher moments of the distribution.

Similarly, while the mean of the tomographic distribution does carry the majority of the information, the median carries significantly less (see Fig. 12). The reason is that the mean has extra information about the tails of the redshift space distribution while the median does not. This sensitivity to the tails will make obtaining precise measurements of the mean difficult. One still requires a fair sample from each of the tomographic redshift bins extending to high redshift. In the end, mean priors require a similar number of training set galaxies as above.

5. DISCUSSION

We have performed a systematic study of the effects of imperfect photometric redshifts on weak-lensing tomography. Describing the photo-z distribution with a bias and scatter that can

vary arbitrarily between redshift intervals of $\delta z = 0.1$, we studied the degeneracies between photo-z and dark energy parameters, as well as the resulting degradations in dark energy parameter errors.

Not surprisingly, we find that there exist significant degeneracies between the dark energy and photo-z parameters. Assuming that the overall distribution of galaxies $n(z)$ is independently known and the photometric redshifts are used only for tomographic subdivision, we find that larger dark energy spaces suffer more degeneracy with photo-z than the smaller ones.

Without any information on photo-z parameters, one recovers the no-tomography case where errors on fiducial parameters are a factor of 2 times worse (for the $\{w_0, \Omega_{DE}\}$ parameterization) or 10 times worse (for the $\{w_0, w_a, \Omega_{DE}\}$ parameterization) than those for the 10 bin tomography case with perfect photo-z's.

For the fiducial survey, in order to have less than a factor of 1.5 degradation in dark energy parameter errors, the uncertainties of photo-z parameters z_{bias} and σ_z (defined in the redshift interval $\delta z = 0.1$) should each be controlled to better than 0.003–0.01, depending again on the size of dark energy parameter space. We provide a convenient approximation for scaling these requirements to different surveys. Importantly, no single number such as the mean or median of galaxies in the tomographic bin captures all of the effect of photo-z errors. That the mean captures more of the information than the median indicates that the dark energy information is sensitive to the tails of the distribution.

In order to achieve less than a factor of 1.5 degradation in the evolution of the equation of state, a training set of a few times 10^4 galaxies with spectroscopic redshifts is required. Again, one can easily rescale the number of galaxy requirements to different surveys using our scaling relation.

There are several caveats to our assessment that merit future study. Although our parameterization can handle photo-z degeneracies, for example, from multiple galaxy types, that lead to bimodality and catastrophic errors, we have limited our study to fiducial models around which their effects are small. Such effects will increase the required number of training set galaxies. Moreover, we have assumed that the parent redshift distribution of the survey is known and that photometric redshifts are only employed to subdivide the galaxy sample for tomography. Uncertainties in the parent distribution can further degrade dark energy determinations.

On the other hand, uncertainties in the parent distribution are also constrained by the training set. If one assumes that $n(z)$ is a smooth function that is parameterized by relatively few parameters, uncertainties in the parent distribution should be smaller than those of the tomographic bins. For illustrative purposes, if we parameterize $n(z)$ with the three parameters of equation (2), we find that the constraint on $n(z)$ from N_{spec}^μ is good enough to have dark energy parameter errors differ by less than 10% from the case where $n(z)$ is fixed.

Given the current state-of-the-art of photo-z algorithms, as well as expected improvements with multiwavelength observations of all source galaxies, prospects for sufficiently accurate determination of photometric redshifts are bright. Nevertheless, it will be an important and challenging task to achieve good control of the photo-z accuracy for the specific types of galaxies selected in lensing surveys and then propagate the remaining photo-z errors into the final cosmological constraints.

REFERENCES

Aldering, G., et al. 2004, PASP, submitted (astro-ph/0405232)
Bacon, D. J., Refregier, A. R., & Ellis, R. S. 2000, MNRAS, 318, 625
Bartelmann, M., & Schneider, P. 2001, Phys. Rep., 340, 291
Bernstein, G., & Jarvis, B. 2002, AJ, 123, 583
Brown, M. L., Taylor, A. N., Bacon, D. J., Gray, M. E., Dye, S., Meisenheimer, K., & Wolf, C. 2003, MNRAS, 341, 100
Dodelson, S., & Zhang, P. 2005, preprint (astro-ph/0501063)
Eisenstein, D. J., & Hu, W. 1999, ApJ, 511, 5
Hagan, B., Ma, C.-P., & Kravtsov, A. 2005, ApJ, 633, 537
Heitmann, K., Ricker, P. M., Warren, M. S., & Habib, S. 2005, ApJS, 160, 28
Heymans, C., et al. 2005, MNRAS, 361, 160
Hirata, C., & Seljak, U. 2003, MNRAS, 343, 459
Hoekstra, H. 2004, MNRAS, 347, 1337
Hoekstra, H., Yee, H., & Gladders, M. 2002, ApJ, 577, 595
Hu, W. 1999, ApJ, 522, L21
———. 2002a, Phys. Rev. D, 65, 023003
———. 2002b, Phys. Rev. D, 66, 083515
Hu, W., & Kravtsov, A. 2003, ApJ, 584, 702
Hu, W., & Tegmark, M. 1999, ApJ, 514, L65
Huterer, D. 2002, Phys. Rev. D, 65, 063001
Huterer, D., & Takada, M. 2005, Astropart. Phys., 23, 369
Huterer, D., Takada, M., Bernstein, G., & Jain, B. 2005, MNRAS, submitted (astro-ph/0506030)
Huterer, D., & White, M. 2005, Phys. Rev. D, 72, 043002
Ishak, M. 2005, MNRAS, 363, 469
Ishak, M., & Hirata, C. M. 2005, Phys. Rev. D, 71, 023002

Jarvis, M., Bernstein, G., Jain, B., Fischer, P., Smith, D., Tyson, J. A., & Wittman, D. 2003, AJ, 125, 1014
Jarvis, M., & Jain, B. 2004, ApJ, submitted (astro-ph/0412234)
Jarvis, M., Jain, B., Bernstein, G., & Dolney, D. 2005, preprint (astro-ph/0502243)
Kaiser, N. 1992, ApJ, 388, 272
———. 1998, ApJ, 498, 26
Kaiser, N., Wilson, G., & Luppino, G. A. 2000, preprint (astro-ph/0003338)
Peacock, J. A., & Dodds, S. J. 1996, MNRAS, 280, L19
Pen, U.-L., van Waerbeke, Y., & Mellier, Y. 2002, ApJ, 567, 31
Pen, U.-L., et al. 2003, ApJ, 592, 664
Refregier, A. 2003, ARA&A, 41, 645
Refregier, A., et al. 2004, AJ, 127, 3102
Song, Y.-S., & Knox, L. 2004, Phys. Rev. D, 70, 063510
Spergel, D. N., et al. 2003, ApJS, 148, 175
Takada, M., & Jain, B. 2004, MNRAS, 348, 897
Vale, C., Hoekstra, H., van Waerbeke, L., & White, M. 2004, ApJ, 613, L1
Vale, C., & White, M. 2003, ApJ, 592, 699
Van Waerbeke, L., Mellier, Y., & Hoekstra, H. 2005, A&A, 429, 75
Van Waerbeke, L., et al. 2000, A&A, 358, 30
White, M. 2004, Astropart. Phys., 22, 211
———. 2005, Astropart. Phys., 23, 349
White, M., & Hu, W. 2000, ApJ, 537, 1
White, M., & Vale, C. 2004, Astropart. Phys., 22, 19
Wittman, D., Tyson, J. A., Kirkman, D., Dell'Antonio, I., & Bernstein, G. 2000, Nature, 405, 143
Zhan, H., & Knox, L. 2004, ApJ, 616, L75